Joint Range and Doppler Adaptive Processing for CBM based DFRC systems

Jifa Zhang

***Abstract*—Recently, dual-function radar communication (DFRC) systems have been proposed to integrate radar and communication into one platform for spectrum sharing. Various signalling strategies have been proposed to embed communication information into the radar transmitted waveforms. Among these, complex beampattern modulation (CBM) embeds communication information into the complex transmit beampattens via changing the amplitude and phase of the beampatterns towards the communication receiver. The embedding of random communication information causes the clutter modulation and high range-Doppler sidelobe. What's more, transmitting different waveforms on a pulse to pulse basis degrades the radar target detection capacity when traditional sequential pulse compression (SPC) and moving-target detection (MTD) is utilized. In this paper, a minimum mean square error (MMSE) based filter, denoted as joint range and Doppler adaptive processing (JRDAP) is proposed. The proposed method estimates the targets' impulse response coefficients at each range-Doppler cell adaptively to suppress high range-Doppler sidelobe and clutter modulation. The performance of proposed method is very close to the full-dimension adaptive multiple pulses compression (AMPC) while reducing computational complexity greatly.**

***Index Terms*—Complex beampattern modulation, Dual-function radar communication, Joint range and Doppler adaptive processing, Minimum mean square error.**

I. Introduction

The competition between radar and communication for scarce spectrum resources has become more and more fierce recently. Spectrum sharing has been proposed to mitigate the competition of radar and communications for spectrum [1]–[3]. Spectrum sharing is roughly divided into co-existence and co-design. The focus of co-existence is to mitigate the interference between radar and communication [4], [5]. And the focus of co-design is the shared waveform design in order to embed communication information into radar emission or embed sensing into communication signal [6], [7]. Dual-function radar communication (DFRC) systems, where the radar and communication are integrated into one platform, is a classical example of co-design [8]. The DFRC systems have the advantages of low cost, compact size, improved performance and safety. There are many applications for DFRC systems, such as defence, internet of vehicles [9]–[11] and autonomous vehicles [12], which is the main focus of this paper.

As for the DFRC systems, where the radar is regarded as the primary function and communication is regarded as the secondary function, many signal embedding strategies, such as complex beampattern modulation (CBM) [13], [14], index modulation (IM) [15], [16], spatial modulation (SM) [17], fast time modulation [18], have been proposed. The essence of CBM is to steer the mainlobe towards the targets of interest while changing the complex beampattern towards the communication receiver according to the random communication symbols. And the communication symbols are represented by specific complex beampatterns towards the communication direction, such as sidelobe levels (SLLs), phases or both. In [19], a phase modulation (PM) based DFRC system was proposed where the communication symbols are represented by specific phases towards communication direction. A quadrature amplitude modulation (QAM) based DFRC system was proposed [20]. As for the IM, the communication symbols are embedded into specific antenna indexes, frequency indexes or phase indexes. The communication symbols are represented by specific radar waveforms for fast time modulation, such as waveform diversity.

As for the waveform diversity based DFRC systems, the transmitted waveforms change on a pulse to pulse basis to deliver random communication information, which causes range sidelobe modulation (RSM) and degrades the target detection capacity of radar when traditional sequential pulse compression (SPC) and moving-target detection (MTD) is utilized [21]. Lots of methods have been proposed to solve the RSM caused by waveform diversity [22]–[27]. In [22], the authors proposed an adaptive pulse compression (APC) method where the targets' impulse response coefficients are estimated adaptively via minimum mean square error (MMSE) estimation. In [23], a MMSE based adaptive multiple pulses compression (AMPC) was proposed to suppress both range and Doppler sidelobes. In [24], a non-identical multiple pulses compression was proposed to mitigate the clutter. The authors proposed a joint least squares (JLS) mismatch filter to achieve nearly identical range sidelobe responses [27]. In [25], the JLS mismatch filter was adopted to moving-target indication (MTI) radar. However, all these methods are restricted to pure radar systems and not applicable to DFRC systems.

Like the waveform diversity, the transmitted waveforms of the CBM based DFRC systems change on a pulse to pulse basis to synthesize specific beampatterns causing the range-Doppler sidelobe modulation. What's more, the clutter located in different azimuth bins are modulated by different complex scale causing clutter modulation [28]. In order to analyse the effect of clutter, knowledge-aided radar systems [29]–[32], where the radar systems have access to some prior information of a dynamic environmental database, such as a geographical information system (GIS), tracking files,

Jifa Zhang is with the School of Electronic and Information Engineering, Beihang University, Beijing 100191, China, E-mail: (jifazhang@yeah.net)

meteorological information and interference models, have been proposed recently.

In this paper, we assume the clutter impulse responses obey the Gaussian distribution and the clutter is assumed as stationary clutter, i.e., the normalized Doppler frequency of the clutter is zero. We first analyse the range-Doppler sidelobe modulation and clutter modulation of DFRC systems due to information embedding. Then, we review the full-dimension AMPC for mitigating range-Doppler sidelobe modulation. Finally, a novel method based on MMSE framework is proposed to mitigate the range-Doppler sidelobe modulation and clutter modulation for CBM based DFRC systems. The proposed method, named by joint range and Doppler adaptive processing (JRDAP), is adopted to replace traditional SPC and MTD (SPC & MTD). In JRDAP, a joint range and Doppler adaptive filter based on MMSE framework is designed to estimate the targets' refection coefficients in each range-Doppler cell under clutter and noise situation. Since the computational complexity of full-dimension AMPC is very high [33], the proposed JRDAP is a dimensionality reduction algorithm, which computational complexity is lower than the full-dimension AMPC.

The contributions of this paper are listed as below:

- Firstly, we analyse the range-Doppler sidelobe modulation and clutter modulation of DFRC systems due to information embedding.
- Secondly, we derive the full-dimension AMPC for DFRC systems based on MMSE framework to mitigate the range-Doppler sidelobe modulation and clutter modulation.
- Finally, we propose a joint range and Doppler adaptive processing, which computational complexity is lower than that of full-dimension AMPC and performance is very close to the full-dimension AMPC.

The rest of this paper is organized as below. The CBM based signaling strategy is reviewed in Section II. The signal model is described in section III. The adaptive multiple pulses compression is presented in section IV. And the proposed JRDAP is described in section V. Simulation results are presented in Section VI and conclusions are drown in Section VII.

Notations: In this paper, the matrices and vectors are denoted by bold uppercase letters (i.e. $\mathbf{A}$) and lowercase letters (i.e. $\mathbf{a}$), respectively. The transpose and the conjugate operation are $(\cdot)^T$ and $(\cdot)^H$, respectively. $\otimes$ denotes the Kronecker product. $\mathbb{C}^N$ denotes the set of N-dimensional vectors of complex numbers. $\mathbf{I}$ denotes the identity matrix, whose dimension is determined by the context. $\mathbb{E}\{\cdot\}$ denotes the mathematical expectation, $|\cdot|$ denotes the module of a complex number and a^* denotes the conjugate of a. $\|\mathbf{x}\|$ denotes the Euclidean norm of the vector $\mathbf{x}$. $\mathbf{B}^{-1}$ denotes the inverse matrix of the invertible matrix $\mathbf{B}$. j denotes the imaginary unit. $\max(a,b)$ returns the larger of a and b. $\mathrm{tr}(\cdot)$ denotes the trace of the matrix argument.

II. Complex Beampattern Modulation Based Signaling Strategy

The CBM signalling strategy, which modulates the transmitted complex beampatterns towards the communication direction, is widely utilized in DFRC systems. In this section, we give a brief review of the CBM signaling strategy.

Suppose a DFRC platform is equipped with a M-element uniform linear array (ULA) with inter-element spacing of half wavelength for transmit and an omnidirectional antenna for receive. We aim to minimize the peak sidelobe level (PSL) and keep the specific complex beampatterns towards the targets of interest and the single communication receiver. The kth beamforming weight vector for the CBM-based signalling strategy can be obtained by solving the following optimization problem:

$$\mathcal{P}_1 \begin{cases} \min_{\tilde{\mathbf{w}}_k,\epsilon} & \epsilon^2 \\ \text{subject to} & |\tilde{\mathbf{w}}_k^H \mathbf{a}(\theta)|^2 \le \epsilon^2 \quad \theta \in \bar{\mathbf{\Theta}} \\ & \tilde{\mathbf{w}}_k^H \mathbf{a}(\theta_t) = 1 \\ & \tilde{\mathbf{w}}_k^H \mathbf{a}(\theta_c) = \Delta_k e^{j\phi_k}, \quad 1 \le k \le K \end{cases} \tag{1}$$

where $\bar{\mathbf{\Theta}}$ denotes the radar sidelobe region, $\mathbf{a}(\theta_t) = [1, e^{-j2\pi\frac{d}{\lambda}\sin\theta_t}, e^{-j2\pi\frac{2d}{\lambda}\sin\theta_t}, \cdots, e^{-j2\pi(M-1)\frac{d}{\lambda}\sin\theta_t}]^T$ and $\mathbf{a}(\theta_c) = [1, e^{-j2\pi\frac{d}{\lambda}\sin\theta_c}, \cdots, e^{-j2\pi(M-1)\frac{d}{\lambda}\sin\theta_c}]^T$ denotes the steering vector of the target and communication receiver, θ_t and θ_c denotes the direction of the target and communication receiver, and $\tilde{\mathbf{w}}_k$ is the kth beamforming weight vector to form the beampattern whose phase and sidelobe level (SLL) towards the communication receiver are ϕ_k and Δ_k, respectively. Each SLL Δ_k and phase ϕ_k are chosen from the predefined dictionary Ω contained L_1 allowable SLLs and Q_1 phases. Therefore, the total number of communication symbols which can be embedded through the CBM is $K = L_1 Q_1$. The optimization problem $\mathcal{P}_1$ is convex [34], and can be solved by off-the-shelf optimization solvers, such as CVX.

III. Signal Model

The range processing window length is L and Q discrete Doppler cells are considered in this paper. Suppose N_c discrete clutter patches are evenly distributed in the angle interval $[-60°, 60°]$ and the clutter is assumed to be stationary clutter, i.e., the Doppler frequency of clutter patches is zero. Consider the DFRC system transmits a burst of P slow-time pulses in a coherent processing interval (CPI). The transmitted weight matrix $\mathbf{W} = [\mathbf{w}_1, \mathbf{w}_2, \cdots, \mathbf{w}_P] \in \mathbb{C}^{M\times P}$ modulates the radar pulses in a CPI. Each column vector of $\mathbf{W}$ is chosen from the K vectors obtained by solving $\mathcal{P}_1$.

The Swerling-I target model is adopted in this paper. What's more, we assume that the reflection coefficients of targets are stationary during the P consecutive pulse transmissions. Therefore, the ℓth sample during the pth pulse can be expressed as

$$\begin{aligned} y_p(\ell) = &\sum_{q=0}^{Q-1} \mathbf{x}^T(\ell,q)\mathbf{s}e^{j2\pi(p-1)\psi_q} \\ &+ \sum_{i=1}^{N_c} \mathbf{w}_p^H \mathbf{a}(\theta_i)\mathbf{c}_i^T(\ell)\mathbf{s} + n_p(\ell), \end{aligned} \tag{2}$$

where $\mathbf{s} = [s(0), s(1), \cdots, s(N-1)]^T$ denotes the samples of transmitted waveform, $\ell = 1, \cdots, L$, $p = 1, 2\cdots, P$, $\mathbf{x}(\ell,q) = [x(\ell,q), x(\ell-1,q), \cdots, x(\ell-N+1,q)]^T$ are N contiguous samples of the range profile impulse response

corresponding to the normalized Doppler frequency $\psi_q = -0.5 + \frac{q-1}{Q}$ ($\psi_q \in [-0.5, 0.5]$) for $q = 1, \cdots, Q$. $\mathbf{c}_i(\ell) = [c_i(\ell), \cdots, c_i(\ell - N + 1)]^T$ denotes N contiguous samples of the clutter impulse response of stationary clutter patch located in ith azimuth bin and $n_p(\ell)$ denotes the noise sample.

Let $\mathbf{y}_p(\ell) = [y_p(\ell), \cdots, y_p(\ell + N - 1)]^T$ denotes the N contiguous samples of $y_p(\ell)$ and the matched filter output of $\mathbf{y}_p(\ell)$ can be formulated as

$$y_{mf,p}(\ell) = \mathbf{s}^H \left(\sum_{q=0}^{Q-1} \mathbf{A}^T(\ell, q) e^{j2\pi(p-1)\psi_q} \right) \mathbf{s} + \mathbf{s}^H \left(\sum_{i=1}^{N_c} \mathbf{w}_p^H \mathbf{a}(\theta_i) \mathbf{C}_i^T(\ell) \right) \mathbf{s} + \tilde{n}_p(\ell), \tag{3}$$

for $p = 1, 2, \cdots, P$, and

$$\mathbf{A}(\ell, q) = \begin{bmatrix} x(\ell, q) & \cdots & x(\ell + N - 1, q) \\ x(\ell - 1, q) & \cdots & x(\ell + N - 2, q) \\ \vdots & \ddots & \vdots \\ x(\ell - N + 1, q) & \cdots & x(\ell, q) \end{bmatrix}, \tag{4}$$

is a set of N length-N sample-shifted snapshots of the impulse response and

$$\mathbf{C}_i(\ell) = \begin{bmatrix} c_i(\ell) & \cdots & c_i(\ell + N - 1) \\ c_i(\ell - 1) & \cdots & c_i(\ell + N - 2) \\ \vdots & \ddots & \vdots \\ c_i(\ell - N + 1) & \cdots & c_i(\ell) \end{bmatrix}, \tag{5}$$

is a set of N length-N sample-shifted snapshots of the impulse response of stationary clutter patch located ith azimuth bin.

Besides, $\mathbf{n}_p(\ell) = [n_p(\ell), \cdots, n_p(\ell + N - 1)]^T$ is the N noise samples and $\tilde{n}_p(\ell) = \mathbf{s}^H \mathbf{n}_p(\ell)$.

When non complex beampattern modulation (NCBM) is utilized, $y_{mf,p}(\ell)$ can be reformulated as

$$y_{mf,p}(\ell) = \mathbf{s}^H \left(\sum_{q=0}^{Q-1} \mathbf{A}^T(\ell, q) e^{j2\pi(p-1)\psi_q} \right) \mathbf{s} + \mathbf{s}^H \left(\sum_{i=1}^{N_c} \mathbf{w}_1^H \mathbf{a}(\theta_i) \mathbf{C}_i^T(\ell) \right) \mathbf{s} + \tilde{n}_p(\ell). \tag{6}$$

Comparing Eq. (3) with Eq. (6), we can observe that the communication embedding modulates clutter through the term $\mathbf{w}_p^H \mathbf{a}(\theta_i)$ cross different pulses in a CPI resulting in the undesired spreading of the clutter spectrum and clutter modulation. Due to the waveform diversity, the traditional SPC & MTD has high range-Doppler sidelobe causing the small targets (low SINR) masked by the large nearby targets (high SINR).

IV. Adaptive multiple pulses compression

In order to compress the range-Doppler sidelobe, full-dimension AMPC is proposed to replace the traditional SPC & MTD [23]. In AMPC, a MMSE filter is utilized to estimate the targets' impulse response coefficients at each range-Doppler cell. The output of MMSE filter at ℓth range cell and qth Doppler cell is given by

$$\hat{x}(\ell, q) = \mathbf{h}^H(\ell, q) \mathbf{y}(\ell), \tag{7}$$

where $\hat{x}(\ell, q)$ denotes the MMSE filter estimate of the ℓth delayed sample of a length-L section of the range profile response corresponding to qth Doppler cell, $\mathbf{h}(\ell, q) = [h_{11}(\ell, q), \cdots, h_{1N}(\ell, q), h_{21}(\ell, q), \cdots, h_{PN}(\ell, q)]^T \in \mathbb{C}^{NP \times 1}$ is the wight vector of MMSE filter corresponding to ℓth range cell and qth Doppler cell, and $\mathbf{y}(\ell)$ is given by

$$\begin{aligned} \mathbf{y}(\ell) &= \left[\mathbf{y}_1^T(\ell), \mathbf{y}_2^T(\ell), \cdots, \mathbf{y}_P^T(\ell) \right]^T \\ &= \begin{bmatrix} \sum_{q=0}^{Q-1} \mathbf{A}^T(\ell, q) \\ \vdots \\ \sum_{q=0}^{Q-1} \mathbf{A}^T(\ell, q) e^{j2\pi(P-1)\psi_q} \end{bmatrix} \mathbf{s} \\ &\quad + \sum_{i=1}^{N_c} \begin{bmatrix} \mathbf{w}_1^H \mathbf{a}(\theta_i) \mathbf{C}_i^T(\ell) \\ \vdots \\ \mathbf{w}_P^H \mathbf{a}(\theta_i) \mathbf{C}_i^T(\ell) \end{bmatrix} \mathbf{s} + \begin{bmatrix} \mathbf{n}_1 \\ \vdots \\ \mathbf{n}_P \end{bmatrix}, \end{aligned} \tag{8}$$

where $\mathbf{y}_i(\ell)$ denotes the vector of N contiguous samples of the received signal during ith pulse for $i = 1, \cdots, P$, $\mathbf{n}_i = [n_i(\ell), \cdots, n_i(\ell + N - 1)]$ denotes the noise vector for $i = 1, 2, \cdots, P$. The cost function for MMSE filter at ℓth range cell and qth Doppler cell is given by

$$\mathcal{J}(\ell, q, \mathbf{h}(\ell, q)) = \mathbb{E}\left[|x(\ell, q) - \mathbf{h}^H(\ell, q) \mathbf{y}(\ell)|^2 \right]. \tag{9}$$

The MMSE cost function $\mathcal{J}(\ell, q, \mathbf{h}(\ell, q))$ is minimized by differentiating with respect to $\mathbf{h}^*(\ell, q)$ and setting the result is equal to zero. Therefore, the optimal $\tilde{\mathbf{h}}(\ell, q)$ takes the following form

$$\tilde{\mathbf{h}}(\ell, q) = \left(\mathbb{E}\{\mathbf{y}(\ell) \mathbf{y}^H(\ell)\} \right)^{-1} \mathbb{E}\{\mathbf{y}(\ell) x^*(\ell, q)\}. \tag{10}$$

We assume the neighboring target impulse response terms are uncorrelated, and the target impulse response terms are uncorrelated with clutter impulse response terms and noise terms too [23]. Therefore, the cross-correction vector can be formulated as

$$\mathbb{E}\left\{ \mathbf{y}(\ell) x^*(\ell, q) \right\} = \rho(\ell, q) [\mathbf{s}^T, \mathbf{s}^T e^{j2\pi\psi_q}, \cdots, \mathbf{s}^T e^{j2\pi(P-1)\psi_q}]^T, \tag{11}$$

where $\rho(\ell, q) = \mathbf{E}\{|x(\ell, q)|^2\}$ denotes the power of $x(\ell, q)$. However, it's impossible to known the impulse response coefficient at the (ℓ, q)th range-Doppler cell. Therefore, the traditional SPC & MTD is utilized to obtain the initial estimation of $\rho(\ell, q)$ firstly. Followed by that, the MMSE filter is performed on the received signal to obtain the enhance estimation taking the initial estimation of $\rho(\ell, q)$ as a prior information.

What's more, we assume that the clutter impulse response terms obey Gaussian distribution and identically distributed (IID), i.e., $\mathbb{E}\{|c(\ell, q)|^2\} = \sigma_c^2, \forall \ell, q$, where σ_c^2 denotes the power of the clutter. Therefore, $\mathbb{E}\{\mathbf{y}(\ell) \mathbf{y}^H(\ell)\} \in \mathbb{C}^{NP \times NP}$ is given by

$$\mathbb{E}\left\{ \mathbf{y}(\ell) \mathbf{y}^H(\ell) \right\} = \mathbf{R}_t(\ell) + \mathbf{R}_c + \mathbf{R}_n, \tag{12}$$

where the signal covariance matrix $\mathbf{R}_t(\ell) \in \mathbb{C}^{NP \times NP}$ is given by

$$\mathbf{R}_t(\ell) = \begin{bmatrix} \mathbf{R}_{t,1,1}(\ell) & \cdots & \mathbf{R}_{t,1,P}(\ell) \\ \vdots & \ddots & \vdots \\ \mathbf{R}_{t,P,1}(\ell) & \cdots & \mathbf{R}_{t,P,P}(\ell) \end{bmatrix}. \tag{13}$$

Lemma 4.1: The (l_1, l_2) element of $\mathbf{R}_t(\ell)$ is formulated as

$$\mathbf{R}_{t,l_1,l_2}(\ell) = \sum_{q=0}^{Q-1} \mathbf{\Phi}(\ell, q) e^{j2\pi(l_1-l_2)\psi_q}, \tag{14}$$

where $\mathbf{\Phi}(\ell, q) = \sum_{n=-N+1}^{N-1} \rho(n+\ell, q)\mathbf{s}_n\mathbf{s}_n^H$, $\mathbf{s}_n$ denotes the transmitted waveform shifted by n samples and the remainder is filled with zero, e.g., $\mathbf{s}_2 = [0, 0, s(0), s(1), \cdots, s(N-3)]^T$ when $n = 2$, and $\mathbf{s}_{-2} = [s(2), \cdots, s(N-1), 0, 0]^T$ when $n = -2$.

Proof 4.1: See Appendix A.

In Eq. (12), $\mathbf{R}_c$ denotes the clutter covariance matrix and is given by

$$\mathbf{R}_c = \begin{bmatrix} \mathbf{R}_{c,1,1} & \cdots & \mathbf{R}_{c,1,P} \\ \vdots & \ddots & \vdots \\ \mathbf{R}_{c,P,1} & \cdots & \mathbf{R}_{c,P,P} \end{bmatrix}. \tag{15}$$

Lemma 4.2: The (l_1, l_2) element of $\mathbf{R}_c$ is formulated as

$$\mathbf{R}_{c,l_1,l_2} = \sum_{i=1}^{N_c} \mathbf{w}_{l_1}^H \mathbf{a}(\theta_i)(\mathbf{w}_{l_2}^H \mathbf{a}(\theta_i))^H \mathbf{\Upsilon}, \tag{16}$$

where $\mathbf{\Upsilon} = \sum_{n=-N+1}^{N-1} \sigma_c^2 \mathbf{s}_n\mathbf{s}_n^H$.

Proof 4.2: See Appendix B.

In Eq. (12), $\mathbf{R}_n$ denotes the noise covariance matrix and the (l_1, l_2) element of $\mathbf{R}_n$ is formulated as

$$\mathbf{R}_{n,l_1,l_2} = \mathbb{E}\{\mathbf{n}_{l_1}\mathbf{n}_{l_2}^H\} = \begin{cases} \sigma_n^2\mathbf{I}, & \text{if } l_1 = l_2 \\ \mathbf{0}, & \text{otherwise.} \end{cases} \tag{17}$$

Therefore, $\mathbf{R}_n = \sigma_n^2\mathbf{I}$, where σ_n^2 denotes the noise power.

However, the computational complexity of the full-dimension AMPC is very high because the computational complexity of $NP \times NP$ matrix inversion in Eq. (10) is very high. Therefore, the use of AMPC is limited for real-time systems. In next section, we propose a dimensionality reduction method, denoted as JRDAP, which can decease the computational complexity greatly.

V. Joint Range and Doppler Adaptive Processing

A. Proposed joint Range and Doppler Adaptive Processing

The standard joint range-Doppler matched filter (JRDMF) can be formulated as [24]

$$\hat{\mathbf{h}}(\ell, q) = \mathbf{d}(\psi_q) \otimes \mathbf{s}, \tag{18}$$

where $\mathbf{d}(\psi_q) = [1, e^{j2\pi\psi_q}, \cdots, e^{j2\pi(P-1)\psi_q}]^T \in \mathbb{C}^P$ denotes the temporal steering vector corresponding to normalized Doppler frequency ψ_q. Inspired by the structure of Eq. (18), we reformulate the $\mathbf{h}(\ell, q)$ in Eq. (9) as

$$\mathbf{h}(\ell, q) = \mathbf{v}_q^* \otimes \mathbf{u}_\ell, \tag{19}$$

where $\mathbf{v}_q \in \mathbb{C}^P$ denotes the weight vector of Doppler adaptive filter corresponding to qth Doppler cell and $\mathbf{u}_\ell \in \mathbb{C}^N$ denotes the weight vector of range adaptive filer corresponding to ℓth range cell. Therefore, the cost function of MMSE based filter can be formulated equivalently as [35]

$$\tilde{\mathcal{J}}(\ell, q, \mathbf{u}_\ell, \mathbf{v}_q) = \mathbb{E}\left\{|x(\ell, q) - \mathbf{u}_\ell^H \mathbf{Y}(\ell)\mathbf{v}_q|^2\right\}, \tag{20}$$

where $\mathbf{Y}(\ell) = [\mathbf{y}_1(\ell), \mathbf{y}_2(\ell), \cdots, \mathbf{y}_P(\ell)] \in \mathbb{C}^{N\times P}$. It is easy to verify that $\tilde{\mathcal{J}}(\ell, q, \mathbf{u}_\ell, \mathbf{v}_q) = \tilde{\mathcal{J}}(\ell, q, \gamma\mathbf{u}_\ell, \gamma^{-1}\mathbf{v}_q)$ for nonzero constant number γ. As a result, there is scale uncertainty between $\mathbf{u}_\ell$ and $\mathbf{v}_q$. In order to eliminate the scale uncertainty, we make the Euclidean norm of $\mathbf{u}_\ell$ equal to 1 in each iteration. In order to decrease computational complexity, we optimize N-dimensional vector $\mathbf{u}_\ell$ and P-dimensional vector $\mathbf{v}_q$ to minimize the cost function rather than optimize $N \times P$-dimensional vector $\mathbf{h}(\ell, q)$. We propose an effective method which optimizes one of $\mathbf{u}_\ell$ and $\mathbf{v}_q$ when the other is fixed iteratively until the stopping criterion is met. The N-dimensional vector $\mathbf{u}_\ell$ and P-dimensional vector $\mathbf{v}_q$ are utilized to obtain the $N \times P$-dimensional weight vector by Eq. (19). In the following, we omit the subscript of $\mathbf{u}_\ell$ and $\mathbf{v}_q$ for ease of presentation, i.e., $\mathbf{u}_\ell$ is replaced by $\mathbf{u}$ and $\mathbf{v}_q$ is replaced by $\mathbf{v}$.

When $\mathbf{u}$ is fixed, the MMSE cost function $\tilde{\mathcal{J}}(\ell, q, \mathbf{u}, \mathbf{v})$ is a quadratic function with respect to $\mathbf{v}$ and is convex. Therefore, $\tilde{\mathcal{J}}(\ell, q, \mathbf{u}, \mathbf{v})$ is minimized by differentiating with respect to $\mathbf{v}^*$ and then setting the result equal to zero, i.e.,

$$\begin{aligned} \frac{\partial\tilde{\mathcal{J}}(\ell, q, \mathbf{u}, \mathbf{v})}{\partial\mathbf{v}^*} &= \mathbb{E}\left\{-x(\ell, q)\mathbf{Y}^H(\ell)\mathbf{u}\right\} \\ &\quad + \mathbb{E}\left\{\mathbf{Y}^H(\ell)\mathbf{u}\mathbf{u}^H\mathbf{Y}(\ell)\mathbf{v}\right\} \\ &= 0, \end{aligned} \tag{21}$$

thus, the optimal Doppler adaptive filter $\tilde{\mathbf{v}}$ takes the form

$$\tilde{\mathbf{v}} = \left(\mathbb{E}\{\mathbf{Y}^H(\ell)\mathbf{u}\mathbf{u}^H\mathbf{Y}(\ell)\}\right)^{-1}\mathbb{E}\left\{x(\ell, q)\mathbf{Y}^H(\ell)\mathbf{u}\right\}. \tag{22}$$

Since the impulse response of target and clutter are uncorrelated, $\mathbb{E}\{x(\ell, q)\mathbf{Y}^H(\ell)\mathbf{u}\}$ is given by

$$\mathbb{E}\{x(\ell, q)\mathbf{Y}^H(\ell)\mathbf{u}\} = \rho(\ell, q)\begin{bmatrix} \mathbf{s}^H\mathbf{u} \\ \vdots \\ \mathbf{s}^H\mathbf{u}e^{-j2\pi(P-1)\psi_q} \end{bmatrix}. \tag{23}$$

$\mathbb{E}\{\mathbf{Y}^H(\ell)\mathbf{u}\mathbf{u}^H\mathbf{Y}(\ell)\} \in \mathbb{C}^{P\times P}$ is formulated as

$$\mathbb{E}\{\mathbf{Y}^H(\ell)\mathbf{u}\mathbf{u}^H\mathbf{Y}(\ell)\} = \tilde{\mathbf{R}}_t(\ell) + \tilde{\mathbf{R}}_c + \tilde{\mathbf{R}}_n. \tag{24}$$

Lemma 5.1: The (l_1, l_2)th element of $\tilde{\mathbf{R}}_t(\ell)$ can be formulated as

$$\begin{aligned} &\tilde{\mathbf{R}}_{t,l_1,l_2}(\ell) \\ =&\mathbf{u}^H\left(\sum_{q=0}^{Q-1}\mathbf{\Phi}(\ell, q)e^{-j2\pi(l_1-l_2)\psi_q}\right)\mathbf{u}. \end{aligned} \tag{25}$$

Proof 5.1: See Appendix C.

Lemma 5.2: The (l_1, l_2)th element of $\tilde{\mathbf{R}}_c$ can be formulated as

$$\tilde{\mathbf{R}}_{c,l_1,l_2} = \sum_{i=1}^{N_c}\mathbf{a}^H(\theta_i)\mathbf{w}_{l_1}\mathbf{w}_{l_2}^H\mathbf{a}(\theta_i)\mathbf{u}^H\mathbf{\Upsilon}\mathbf{u}. \tag{26}$$

Proof 5.2: See Appendix D.

The (l_1, l_2)th element of $\tilde{\mathbf{R}}_n$ can be formulated as

$$\begin{aligned} \tilde{\mathbf{R}}_{n,l_1,l_2} &= \mathbb{E}\{\mathbf{n}_{l_1}^H\mathbf{u}\mathbf{u}^H\mathbf{n}_{l_2}\} \\ &= \mathbb{E}\{\text{tr}(\mathbf{n}_{l_1}^H\mathbf{u}\mathbf{u}^H\mathbf{n}_{l_2})\} \\ &= \text{tr}\left(\mathbf{u}\mathbf{u}^H\mathbb{E}\left\{\mathbf{n}_{l_2}\mathbf{n}_{l_1}^H\right\}\right), \end{aligned} \tag{27}$$

since

$$\mathbb{E}\left\{\mathbf{n}_{l_2}\mathbf{n}_{l_1}^H\right\} = \begin{cases}\sigma_n^2\mathbf{I}, & \text{if } l_1 = l_2\\ \mathbf{0}, & \text{otherwise.}\end{cases} \tag{28}$$

Therefore, $\tilde{\mathbf{R}}_{n,l_1,l_2}$ is given by

$$\tilde{\mathbf{R}}_{n,l_1,l_2} = \begin{cases}\sigma_n^2\|\mathbf{u}\|^2, & \text{if } l_1 = l_2\\ 0, & \text{otherwise.}\end{cases} \tag{29}$$

thus, $\tilde{\mathbf{R}}_n = \sigma_n^2\|\mathbf{u}\|^2\mathbf{I}$.

When $\mathbf{v}$ is fixed, the MMSE cost function $\tilde{\mathcal{J}}(\ell, q, \mathbf{u}, \mathbf{v})$ is a quadratic function with respect to $\mathbf{u}$ and is convex. Therefore, $\tilde{\mathcal{J}}(\ell, q, \mathbf{u}, \mathbf{v})$ is minimized by differentiating with respect to $\mathbf{u}^*$, then setting the result equal to zero, i.e.,

$$\begin{aligned}\frac{\partial\tilde{\mathcal{J}}(\ell, q, \mathbf{u}, \mathbf{v})}{\partial\mathbf{u}^*} &= \mathbb{E}\left\{-x^*(\ell, q)\mathbf{Y}(\ell)\mathbf{v}\right\}\\ &\quad + \mathbb{E}\left\{\mathbf{Y}(\ell)\mathbf{v}\mathbf{v}^H\mathbf{Y}^H(\ell)\mathbf{u}\right\}\\ &= 0,\end{aligned} \tag{30}$$

thus, the optimal range adaptive filter $\tilde{\mathbf{u}}$ takes the form

$$\tilde{\mathbf{u}} = \left(\mathbb{E}\left\{\mathbf{Y}(\ell)\mathbf{v}\mathbf{v}^H\mathbf{Y}^H(\ell)\right\}\right)^{-1}\mathbb{E}\left\{x^*(\ell, q)\mathbf{Y}(\ell)\mathbf{v}\right\}. \tag{31}$$

Upon assuming neighboring impulse response terms are uncorrelated, $\mathbb{E}\{x^*(\ell, q)\mathbf{Y}(\ell)\mathbf{v}\}$ can be formulated as

$$\mathbb{E}\{x^*(\ell, q)\mathbf{Y}(\ell)\mathbf{v}\} = \rho(\ell, q)[\mathbf{s}, \cdots, \mathbf{s}e^{j2\pi(P-1)\psi_q}]\mathbf{v}, \tag{32}$$

and $\mathbb{E}\{\mathbf{Y}(\ell)\mathbf{v}\mathbf{v}^H\mathbf{Y}^H(\ell)\} \in \mathbb{C}^{N\times N}$ is formulated as

$$\mathbb{E}\left\{\mathbf{Y}(\ell)\mathbf{v}\mathbf{v}^H\mathbf{Y}^H(\ell)\right\} = \bar{\mathbf{R}}_t(\ell) + \bar{\mathbf{R}}_c + \bar{\mathbf{R}}_n. \tag{33}$$

Lemma 5.3: $\bar{\mathbf{R}}_t(\ell)$ can be written as

$$\bar{\mathbf{R}}_t(\ell) = \sum_{q=0}^{Q-1}|\beta_q|^2\mathbf{\Phi}(\ell, q), \tag{34}$$

where $\beta_q = \mathbf{v}(1) + \mathbf{v}(2)e^{j2\pi\psi_q} + \cdots + \mathbf{v}(P)e^{j2\pi(P-1)\psi_q}$.

Proof 5.3: See Appendix E.

Lemma 5.4: $\bar{\mathbf{R}}_c$ can be written as

$$\bar{\mathbf{R}}_c = \sum_{i=1}^{N_c}|\beta_i|^2\mathbf{\Upsilon}, \tag{35}$$

where $\beta_i = \mathbf{v}(1)\mathbf{w}_1^H\mathbf{a}(\theta_i) + \cdots + \mathbf{v}(P)\mathbf{w}_P^H\mathbf{a}(\theta_i)$.

Proof 5.4: See Appendix F.

$\bar{\mathbf{R}}_n$ can be written as

$$\begin{aligned}\bar{\mathbf{R}}_n &= \mathbb{E}\left\{([\mathbf{n}_1, \cdots, \mathbf{n}_P]\mathbf{v})([\mathbf{n}_1, \cdots, \mathbf{n}_P]\mathbf{v})^H\right\}\\ &= \mathbb{E}\left\{\left(\sum_{i=1}^{P}\mathbf{v}(i)\mathbf{n}_i\right)\left(\sum_{m=1}^{P}\mathbf{v}(m)\mathbf{n}_m\right)^H\right\}\\ &= \mathbb{E}\left\{\sum_{i=1}^{P}|\mathbf{v}(i)|^2\mathbf{n}_i\mathbf{n}_i^H\right\}\\ &= \sum_{i=1}^{P}|\mathbf{v}(i)|^2\mathbb{E}\left\{\mathbf{n}_i\mathbf{n}_i^H\right\}\\ &= \sigma_n^2\|\mathbf{v}\|^2\mathbf{I}.\end{aligned} \tag{36}$$

In order to eliminate scale uncertainty, we normalize the vector $\tilde{\mathbf{u}}$ in every iteration. Let $\mathbf{v}^i$ denotes the value of $\mathbf{v}$ at ith iteration and $\mathbf{u}^i$ denotes the value of $\mathbf{u}$ at ith iteration. The iteration rule of proposed method is formulated as below:

$$\mathbf{v}^i = (\mathbb{E}\{\mathbf{Y}^H(\ell)\mathbf{u}^{i-1}\mathbf{u}^{(i-1)H}\mathbf{Y}(\ell)\})^{-1}\mathbb{E}\{x(\ell, q)\mathbf{Y}^H(\ell)\mathbf{u}^{i-1}\}, \tag{37}$$

$$\mathbf{u}^i = \frac{\left(\mathbb{E}\left\{\mathbf{Y}(\ell)\mathbf{v}^i\mathbf{v}^{(i)H}\mathbf{Y}^H(\ell)\right\}\right)^{-1}\mathbb{E}\left\{x^*(\ell, q)\mathbf{Y}(\ell)\mathbf{v}^i\right\}}{\|\left(\mathbb{E}\left\{\mathbf{Y}(\ell)\mathbf{v}^i\mathbf{v}^{(i)H}\mathbf{Y}^H(\ell)\right\}\right)^{-1}\mathbb{E}\left\{x^*(\ell, q)\mathbf{Y}(\ell)\mathbf{v}^i\right\}\|}, \tag{38}$$

for $i = 1, 2, \cdots$. The detailed description of proposed JRDAP is shown in Algorithm 1.

Algorithm 1 Proposed joint range and Doppler adaptive processing method

Input: nonzero normalized vector $\mathbf{u}^0$, η, $\rho(\ell, q)$, G, $x(\ell, q)$, $\mathbf{Y}(\ell)$, $\mathbf{s}$, P, $i = 1$;
Output: $\mathbf{u}^{(i)}$, $\mathbf{v}^{(i)}$;

1: **repeat**
2: Substitute $\mathbf{u}^{i-1}$ into Eq. (37) to obtain $\mathbf{v}^i$;
3: Substitute $\mathbf{v}^i$ into Eq. (38) to obtain $\mathbf{u}^i$;
4: $i = i + 1$;
5: **until** $\|\mathbf{u}^i - \mathbf{u}^{i-1}\| \le \eta$ or reaches the maximum iteration number G;

The output of joint range and Doppler adaptive filter corresponding to ℓth range cell and qth Doppler cell is formulated as

$$\hat{x}(\ell, q) = (\mathbf{v}_q^* \otimes \mathbf{u}_\ell)^H\mathbf{y}(\ell). \tag{39}$$

The JRDAP is utilized to estimate the targets' impulse coefficient in all range-Doppler cells. As can be seen in Eq. (25), Eq. (26), Eq. (34), Eq. (35) some matrices such as $\mathbf{\Upsilon}$, $\sum_{q=0}^{Q-1}\mathbf{\Phi}(\ell, q)e^{j2\pi(l_1-l_2)\psi_q}$ $\forall l_1$, $l_2 \in \{1, \cdots, P\}$ are often utilized, we can calculate these terms before using them to reduce the amount of calculation. The block diagram of JRDAP is shown in Algorithm 2.

Algorithm 2 Block diagram of JRDAP

Input: $\rho(\ell, q)$, $\mathbf{W}$, $\mathbf{y}(\ell)$, L, Q, N_c, σ_c^2, σ_n^2, $\mathbf{s}$, P, G, N;
Output: $\hat{x}(\ell, q)$, $\forall \ell, q$;

1: Calculate matrix $\mathbf{\Upsilon}$;
2: **for** $\ell = 1$; $\ell <= L$; $\ell++$ **do**
3: Calculate matrices $\sum_{q=0}^{Q-1}\mathbf{\Phi}(\ell, q)e^{j2\pi(l_1-l_2)\psi_q}$, $\forall l_1, l_2 \in \{1, \cdots, P\}$;
4: **for** $q = 0$; $q <= Q-1$; $q++$ **do**
5: Calculate $\mathbf{u}_\ell$ and $\mathbf{v}_q$ by utilizing Algorithm 1;
6: $\hat{x}(\ell, q) = (\mathbf{v}_q^* \otimes \mathbf{u}_\ell)^H\mathbf{y}(\ell)$;
7: **end for**
8: **end for**

B. Computational complexity

The computational complexity of AMPC is $\mathcal{O}(N^3P^3)$ and proposed adaptive range filter and Doppler filter is $\mathcal{O}[\hat{L}\max(QP^2N^2, N_cP^2N^2)]$, where $\hat{L}$ denotes the number of iterations. In practice, Q and N_c are far less than $N \times P$. Besides, as shown in Fig. 1, the proposed method converges in two iterations, where the estimation error is defined by

$$\hat{e}^i(\ell, q) = |\bar{x}(\ell, q) - \hat{x}^i(\ell, q)|, \tag{40}$$

where $\bar{x}(\ell,q)$ denotes the target impulse response at (ℓ,q)th range-Doppler cell estimated by SPC & MTD and $\hat{x}^i(\ell,q) = (\mathbf{v}_q^{(i)*} \otimes \mathbf{u}_\ell^i)^H \mathbf{y}(\ell)$ denotes the target impulse response at (ℓ,q)th range-Doppler cell estimated by proposed JRDAP at ith iteration. Therefore, the proposed method is more effective than AMPC.

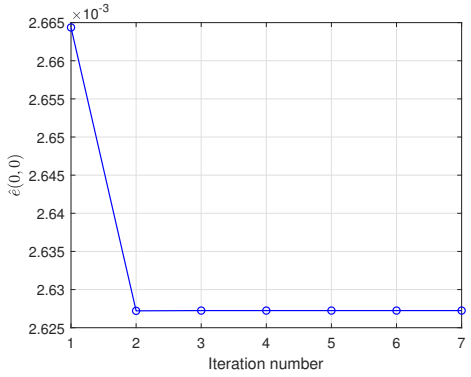

Fig. 1. Convergence of proposed method

C. Convergence

The cost function $\tilde{\mathcal{J}}(\ell,q,\mathbf{u},\mathbf{v})$ given in Eq. (20) is continuous and differentiable. What's more, $\tilde{\mathcal{J}}(\ell,q,\mathbf{u},\mathbf{v}) \geq 0$, i.e., the cost function has a lower bound.

It's evident that Eq. (37) and Eq. (38) are equivalently to solve $\min_{\mathbf{v}} \tilde{\mathcal{J}}(\ell,q,\mathbf{u}^{i-1},\mathbf{v})$ for a fixed $\mathbf{u}^{i-1}$ and solve $\min_{\mathbf{u}} \tilde{\mathcal{J}}(\ell,q,\mathbf{u},\mathbf{v}^i)$ for a fixed $\mathbf{v}^i$, respectively. Therefore, we can obtain

$$\tilde{\mathcal{J}}(\ell,q,\mathbf{u}^{i-1},\mathbf{v}^{i-1}) \geq \tilde{\mathcal{J}}(\ell,q,\mathbf{u}^{i-1},\mathbf{v}^i) = \min_{\mathbf{v}} \tilde{\mathcal{J}}(\ell,q,\mathbf{u}^{i-1},\mathbf{v}) \geq \tilde{\mathcal{J}}(\ell,q,\mathbf{u}^i,\mathbf{v}^i) = \min_{\mathbf{u}} \tilde{\mathcal{J}}(\ell,q,\mathbf{u},\mathbf{v}^i), \tag{41}$$

for $i = 1,2,\cdots$. Eq. (41) implies that $\tilde{\mathcal{J}}(\ell,q,\mathbf{u}^i,\mathbf{v}^i) \leq \tilde{\mathcal{J}}(\ell,q,\mathbf{u}^0,\mathbf{v}^0)$ for $i = 1,2,\cdots$ and the sequence $\{\tilde{\mathcal{J}}(\ell,q,\mathbf{u}^i,\mathbf{v}^i)\}$ is monotonically decreasing. According to Dedekind theorem [36], the sequence $\{\tilde{\mathcal{J}}(\ell,q,\mathbf{u}^i,\mathbf{v}^i)\}$ is convergent.

VI. Simulation Results

In this section, simulation results are presented to illustrate the benefits of the proposed method. The simulation parameters are set as follows unless specified otherwise. The DFRC system is equipped with a 10-element ULA with an inter-element spacing of half-wavelength for transmit and an omnidirectional antenna for receive. In the simulation, the transmit waveform is linear frequency modulation (LFM) waveform with length $N = 32$, pulse width $\tau = 4\mu$s, bandwidth $B = 4$MHz and initial frequency is 1GHz. We assume that $P = 30$ pulses are transmitted during a CPI and the transmitted weight vectors for each pulse is randomly selected from the specially designed dictionary Ω. The length of processing window is set as $L = 80$ and the number of Doppler cell is set as $Q = 64$. It's assumed that there are three moving targets under test. The angle, range cell, Doppler cell and SNR of targets are listed in Table I. The noise power is set as $\sigma_n^2 = 0$dB. The number of clutter patches is $N_c = 100$ and the clutter patches are evenly distributed in the angle interval $[-60°, 60°]$. The clutter to noise ratio (CNR) is set as 28dB. A single communication receiver is located at $\theta_c = -50°$. The sidelobe region of radar is set as $\bar{\mathbf{\Theta}} = [-90°,-5°] \cup [5°, 90°]$. The maximum iteration number is set as $G = 10^3$.

TABLE I
Parameters of Moving Targets

Angle(°)	Range cell	Doppler cell	SNR(dB)
0	35	52	10
0	50	47	5
0	40	52	-5

We assume that 2 bits of communication information are delivered in each radar pulse, i.e., $K = 4$. For the CBM based signalling strategy mentioned above, $L_1 = 2$ communication SLLs of -25dB and -30dB are used, and each level is associated with $Q_1 = 2$ phases of 0 and π radian. Fig. 2 shows the four transmit patterns with different phases and communication SLLs. The four beamforming weight vectors are utilized in the following simulations.

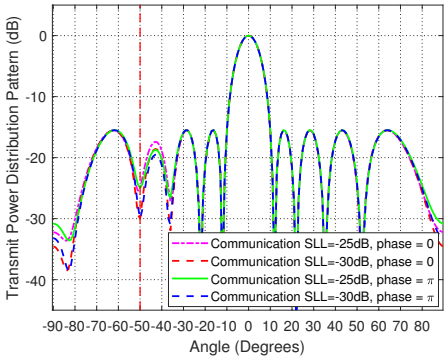

Fig. 2. Transmit beampattern corresponding to the dictionary Ω of weighting vectors $\tilde{\mathbf{w}}_k$

We performance 51200 Monte-carlo simulations using MATLAB softwave on a PC (3.0GHz Intel(R) Core(TM) i7-9700 CPU, 8GB RAM) to compare the average run time per range-Doppler cell of AMPC and JRDAP. The results are listed in Table. II. As shown in Table. II, the average run time of proposed JRDAD is much less than that of AMPC both in CBM and NCBM situation.

As for the clutter free situation, i.e., $N_c = 0$, the range-Doppler map of SPC & MTD, JRDMF, AMPC, and JRDAP are shown in Fig. 3. As shown in the figure, both SPC & MTD and JRDMF suffer high range-Doppler sidelobe, the small target is masked by the nearby large target. For example, the target located the $(40,52)$th range-Doppler cell is masked by the target located the $(35,52)$th range-Doppler cell. What's more, both AMPC and JRDAP can compress range-Doppler sidelobe effectively and all three targets are visible in the range-Doppler map.

The range-Doppler maps of SPC & MTD, JRDMF, AMPC, and JRDAP under clutter and NCBM situation are shown in Fig. 4. The results of SPC & MTD and JRDMF show

that all three targets are masked by the clutter background. On the contrary, two targets with 10dB SNR and 5dB SNR are visible in the range-Doppler maps produced by AMPC and JRDAP while the target with -5dB SNR is masked by the clutter background. What's more, the clutter spectrum becomes narrower and clutter power becomes weaker. As a consequence, the performance of AMPC and JRDAP is much better than SPC & MTD and JRDMF. What's more, the performance of JRDAP is very close to that of AMPC.

The range-Doppler maps of SPC & MTD, JRDMF, AMPC, and JRDAP under clutter and CBM situation are shown in Fig. 5. The results of SPC & MTD and JRDMF show that none of targets are visible due to spreading clutter. However, the two targets with 10dB SNR and 5dB SNR are uncovered from the spreading clutter by AMPC and JRDAP. What's more, the clutter spectrum becomes narrower and clutter power becomes weaker. Therefore, both AMPC and JRDAP can effectively suppress the spreading clutter. What's more, the performance of JRDAP is very close to that of AMPC.

VII. Conclusion

In this paper, we analyzed the effect of CBM on clutter modulation of DFRC systems. The CBM based DFRC systems transmits different waveforms on a pulse to pulse basis causing the clutter modulation and range-Doppler sidelobe modulation. We presented the received signal model of shared waveforms and proposed an effective MMSE based filter to estimate the targets' impulse response coefficients adaptively. Simulation results validated that the proposed MMSE-based filter, named by JRDAP, can suppress the range-Doppler sidelobe and spreading clutter effectively. What's more, performance of proposed JRADP is close to full-dimension adaptive multiple pulses compression but the computational complexity of proposed JRADP is much lower than that of full-dimension adaptive multiple pulses compression.

VIII. Appendix

Appendix A
Proof of Lemma 4.1

$\mathbf{R}_{t,l_1,l_2}(\ell)$ is formulated as

$$\mathbf{R}_{t,l_1,l_2}(\ell) = \mathbb{E}\Bigg\{ \left(\sum_{q=0}^{Q-1} \mathbf{A}^T(\ell,q)\mathbf{s}e^{j2\pi(l_1-1)\psi_q}\right) \times \left(\sum_{m=0}^{Q-1} \mathbf{A}^T(\ell,m)\mathbf{s}e^{j2\pi(l_2-1)\psi_m}\right)^H \Bigg\}. \tag{42}$$

Since the impulse response of targets is uncorrelated with each other, Eq. (42) is formulated as

$$\mathbf{R}_{t,l_1,l_2}(\ell) = \sum_{q=0}^{Q-1} \mathbb{E}\left\{\mathbf{A}^T(\ell,q)\mathbf{s}\mathbf{s}^H\mathbf{A}^*(\ell,q)\right\} e^{j2\pi(l_1-l_2)\psi_q}, \tag{43}$$

Since $\mathbb{E}\left\{\mathbf{A}^T(\ell,q)\mathbf{s}\mathbf{s}^H\mathbf{A}^*(\ell,q)\right\} = \sum_{n=-N+1}^{N-1}\rho(n+\ell,q)\mathbf{s}_n\mathbf{s}_n^H$ [22], Eq. (43) can be formulated as

$$\begin{aligned}\mathbf{R}_{t,l_1,l_2}(\ell) &= \sum_{q=0}^{Q-1}\sum_{n=-N+1}^{N-1}\rho(n+\ell,q)\mathbf{s}_n\mathbf{s}_n^H e^{j2\pi(l_1-l_2)\psi_q} \\ &= \sum_{q=0}^{Q-1}\mathbf{\Phi}(\ell,q)e^{j2\pi(l_1-l_2)\psi_q},\end{aligned} \tag{44}$$

where $\mathbf{\Phi}(\ell,q) = \sum_{n=-N+1}^{N-1}\rho(n+\ell,q)\mathbf{s}_n\mathbf{s}_n^H$.

Appendix B
Proof of Lemma 4.2

$\mathbf{R}_{c,l_1,l_2}$ is formulated as

$$\mathbf{R}_{c,l_1,l_2} = \mathbb{E}\left\{\left(\sum_{i=1}^{N_c}\mathbf{w}_{l_1}^H\mathbf{a}(\theta_i)\mathbf{C}_i^T(\ell)\mathbf{s}\right)\left(\sum_{m=1}^{N_c}\mathbf{w}_{l_2}^H\mathbf{a}(\theta_m)\mathbf{C}_m^T(\ell)\mathbf{s}\right)^H\right\}, \tag{45}$$

since the impulse response of clutter is uncorrelated with each other, Eq. (45) is formulated as

$$\begin{aligned}\mathbf{R}_{c,l_1,l_2} &= \sum_{i=1}^{N_c}\mathbf{w}_{l_1}^H\mathbf{a}(\theta_i)(\mathbf{w}_{l_2}^H\mathbf{a}(\theta_i))^H\mathbb{E}\left\{\mathbf{C}_i^T(\ell)\mathbf{s}\mathbf{s}^H\mathbf{C}_i^*(\ell)\right\} \\ &= \sum_{i=1}^{N_c}\mathbf{w}_{l_1}^H\mathbf{a}(\theta_i)(\mathbf{w}_{l_2}^H\mathbf{a}(\theta_i))^H\sum_{n=-N+1}^{N-1}\sigma_c^2\mathbf{s}_n\mathbf{s}_n^H \\ &= \sum_{i=1}^{N_c}\mathbf{w}_{l_1}^H\mathbf{a}(\theta_i)(\mathbf{w}_{l_2}^H\mathbf{a}(\theta_i))^H\mathbf{\Upsilon},\end{aligned} \tag{46}$$

where $\mathbf{\Upsilon} = \sum_{n=-N+1}^{N-1}\sigma_c^2\mathbf{s}_n\mathbf{s}_n^H$.

Appendix C
Proof of Lemma 5.1

$\tilde{\mathbf{R}}_{t,l_1,l_2}(\ell)$ is formulated as

$$\begin{aligned}\tilde{\mathbf{R}}_{t,l_1,l_2}(\ell) =& \mathbb{E}\Bigg\{\left(\sum_{q=0}^{Q-1}\mathbf{s}^H\mathbf{A}^*(\ell,q)\mathbf{u}e^{-j2\pi(l_1-1)\psi_q}\right) \\ &\times\left(\sum_{m=0}^{Q-1}\mathbf{u}^H\mathbf{A}^T(\ell,m)\mathbf{s}e^{j2\pi(l_2-1)\psi_m}\right)\Bigg\},\end{aligned} \tag{47}$$

TABLE II
COMPARISON OF THE AVERAGE RUN TIME (IN SECONDS).

Algorithm	AMPC & CBM	JRDAP & CBM	AMPC & NCBM	JRDAP & NCBM
Average computational time [s]	0.0682	0.0534	0.0482	0.0449

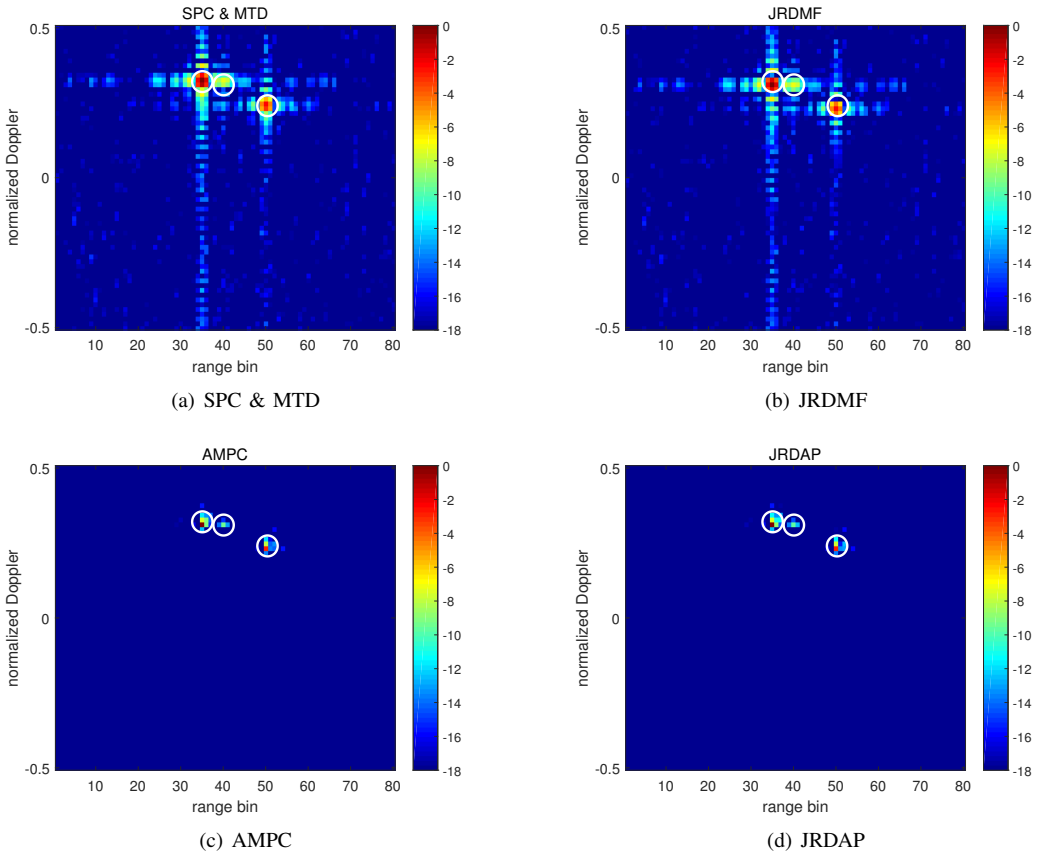

(a) SPC & MTD (b) JRDMF

(c) AMPC (d) JRDAP

Fig. 3. Range-Doppler map in dB of (a) SPC & MTD, (b) JRDMF, (c) AMPC and (d) JRDAP in clutter free; the targets are indicated by the white circles

since the impulse response of targets is uncorrelated with each other, Eq. (47) is formulated as

$$\begin{aligned}
&\tilde{\mathbf{R}}_{t,l_1,l_2}(\ell) \qquad (48)\\
&= \sum_{q=0}^{Q-1} \mathbb{E}\left\{\mathbf{s}^H\mathbf{A}^*(\ell,q)\mathbf{u}\mathbf{u}^H\mathbf{A}^T(\ell,q)\mathbf{s}\right\} e^{-j2\pi(l_1-l_2)\psi_q}\\
&= \mathbf{u}^H\left(\sum_{q=0}^{Q-1} \mathbb{E}\left\{\mathbf{A}^T(\ell,q)\mathbf{s}\mathbf{s}^H\mathbf{A}^*(\ell,q)\right\} e^{-j2\pi(l_1-l_2)\psi_q}\right)\mathbf{u}\\
&= \mathbf{u}^H\left(\sum_{q=0}^{Q-1}\sum_{n=-N+1}^{N-1} \rho(n+\ell,q)\mathbf{s}_n\mathbf{s}_n^H e^{-j2\pi(l_1-l_2)\psi_q}\right)\mathbf{u}\\
&= \mathbf{u}^H\left(\sum_{q=0}^{Q-1} \mathbf{\Phi}(\ell,q)e^{-j2\pi(l_1-l_2)\psi_q}\right)\mathbf{u}.
\end{aligned}$$

APPENDIX D
PROOF OF LEMMA 5.2

$\tilde{\mathbf{R}}_{c,l_1,l_2}$ is formulated as

$$\begin{aligned}
\tilde{\mathbf{R}}_{c,l_1,l_2} = \mathbb{E}\Bigg\{&\left(\sum_{i=1}^{N_c}(\mathbf{w}_{l_1}^H\mathbf{a}(\theta_i))^H\mathbf{s}^H\mathbf{C}_i^*(\ell)\mathbf{u}\right) \qquad (49)\\
&\times\left(\sum_{m=1}^{N_c}\mathbf{w}_{l_2}^H\mathbf{a}(\theta_m)\mathbf{u}^H\mathbf{C}_m^T(\ell)\mathbf{s}\right)\Bigg\}.
\end{aligned}$$

Since the impulse response of clutter is uncorrelated with

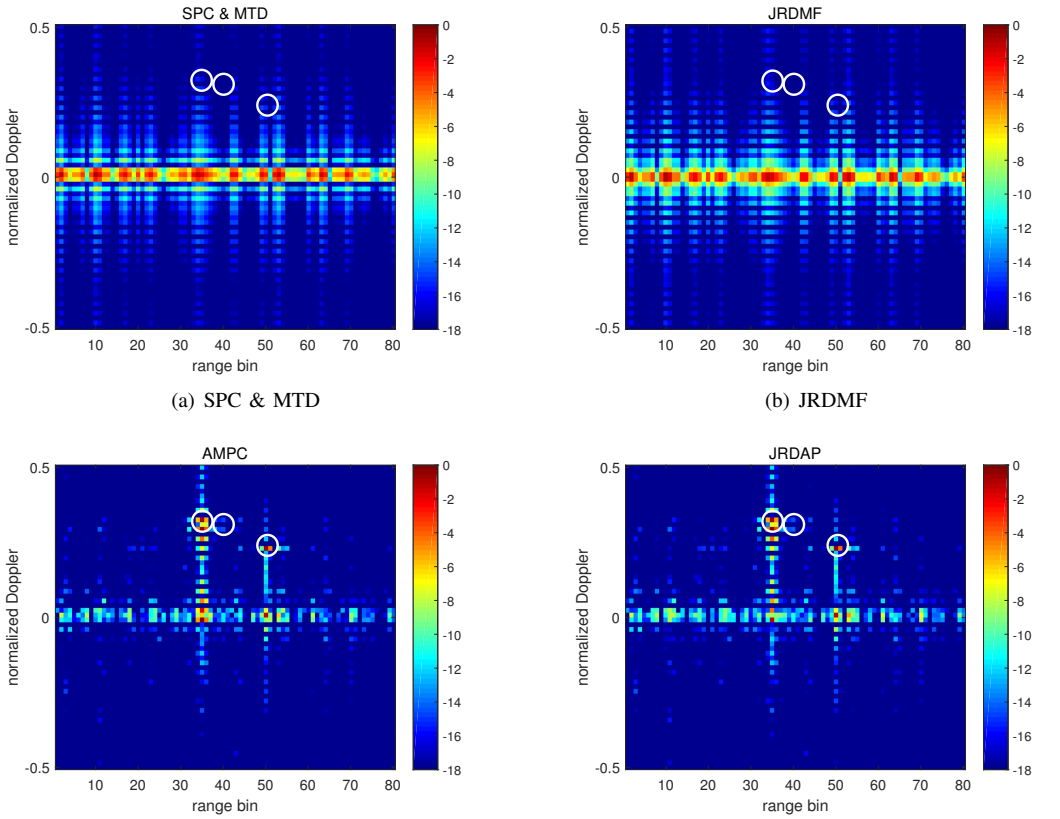

(a) SPC & MTD (b) JRDMF

(c) AMPC (d) JRDAP

Fig. 4. Range-Doppler map in dB of (a) SPC & MTD, (b) JRDMF, (c) AMPC and (d) JRDAP in clutter and NCBM; the targets are indicated by the white circles

each other, Eq. (49) is formulated as

$$\begin{aligned}\tilde{\mathbf{R}}_{c,l_1,l_2} &= \sum_{i=1}^{N_c} \mathbf{a}^H(\theta_i)\mathbf{w}_{l_1}\mathbf{w}_{l_2}^H\mathbf{a}(\theta_i)\mathbb{E}\left\{\mathbf{s}^H\mathbf{C}_i^*(\ell)\mathbf{u}\mathbf{u}^H\mathbf{C}_i^T(\ell)\mathbf{s}\right\} \\ &= \sum_{i=1}^{N_c} \mathbf{a}^H(\theta_i)\mathbf{w}_{l_1}\mathbf{w}_{l_2}^H\mathbf{a}(\theta_i)\mathbb{E}\left\{\mathbf{u}^H\mathbf{C}_i^T(\ell)\mathbf{s}\mathbf{s}^H\mathbf{C}_i^*(\ell)\mathbf{u}\right\} \\ &= \sum_{i=1}^{N_c} \mathbf{a}^H(\theta_i)\mathbf{w}_{l_1}\mathbf{w}_{l_2}^H\mathbf{a}(\theta_i)\mathbf{u}^H\left(\sum_{n=-N+1}^{N-1}\sigma_c^2\mathbf{s}_n\mathbf{s}_n^H\right)\mathbf{u} \\ &= \sum_{i=1}^{N_c} \mathbf{a}^H(\theta_i)\mathbf{w}_{l_1}\mathbf{w}_{l_2}^H\mathbf{a}(\theta_i)\mathbf{u}^H\boldsymbol{\Upsilon}\mathbf{u}.\end{aligned} \tag{50}$$

Appendix E
Proof of Lemma 5.3

$\bar{\mathbf{R}}_t(\ell)$ is formulated as

$$\begin{aligned}&\bar{\mathbf{R}}_t(\ell) \\ =&\mathbb{E}\left\{\left(\sum_{q=0}^{Q-1}(\mathbf{v}(1)+\cdots+\mathbf{v}(P)e^{j2\pi(P-1)\psi_q})\mathbf{A}^T(\ell,q)\mathbf{s}\right)\right. \\ &\left.\times\left(\sum_{m=0}^{Q-1}(\mathbf{v}(1)+\cdots+\mathbf{v}(P)e^{j2\pi(P-1)\psi_m})\mathbf{A}^T(\ell,m)\mathbf{s}\right)^H\right\} \\ =&\mathbb{E}\left\{\sum_{q=0}^{Q-1}|\beta_q|^2\mathbf{A}^T(\ell,q)\mathbf{s}\mathbf{s}^H\mathbf{A}^*(\ell,q)\right\} \\ =&\sum_{q=0}^{Q-1}|\beta_q|^2\mathbb{E}\{\mathbf{A}^T(\ell,q)\mathbf{s}\mathbf{s}^H\mathbf{A}^*(\ell,q)\},\end{aligned} \tag{51}$$

where $\beta_q = \mathbf{v}(1)+\cdots+\mathbf{v}(P)e^{j2\pi(P-1)\psi_q}$. Since $\mathbb{E}\{\mathbf{A}^T(\ell,q)\mathbf{s}\mathbf{s}^H\mathbf{A}^*(\ell,q)\} = \sum_{n=-N+1}^{N-1}\rho(\ell+n,q)\mathbf{s}_n\mathbf{s}_n^H$, Eq. (51) can be formulated as

$$\begin{aligned}\bar{\mathbf{R}}_t(\ell) &= \sum_{q=0}^{Q-1}|\beta_q|^2\sum_{n=-N+1}^{N-1}\rho(\ell+n,q)\mathbf{s}_n\mathbf{s}_n^H \\ &= \sum_{q=0}^{Q-1}|\beta_q|^2\boldsymbol{\Phi}(\ell,q).\end{aligned} \tag{52}$$

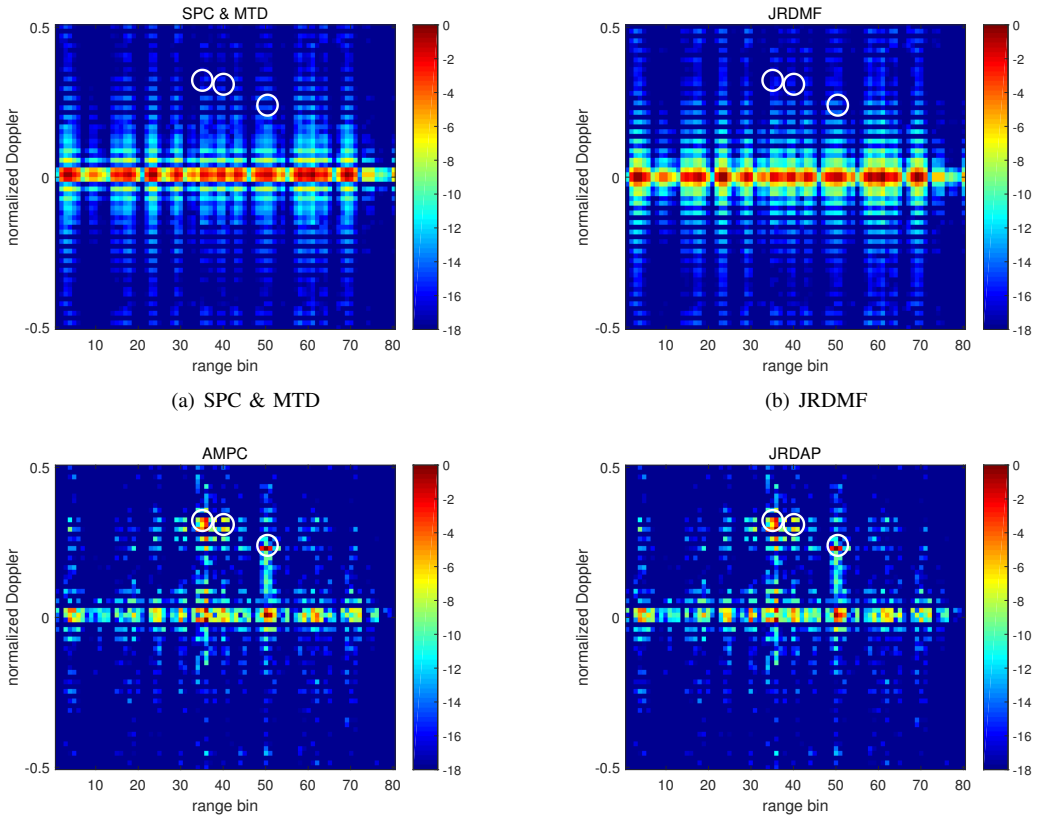

(a) SPC & MTD (b) JRDMF

(c) AMPC (d) JRDAP

Fig. 5. Range-Doppler map in dB of (a) SPC & MTD, (b) JRDMF, (c) AMPC and (d) JRDAP in clutter and CBM; the targets are indicated by the white circles

APPENDIX F
PROOF OF LEMMA 5.4

$\bar{\mathbf{R}}_c$ is formulated as

$$\begin{aligned}&\bar{\mathbf{R}}_c \qquad (53)\\ =&\mathbb{E}\Bigg\{\sum_{i=1}^{N_c}\left((\mathbf{v}(1)(\mathbf{w}_1^H\mathbf{a}(\theta_i))+\cdots+\mathbf{v}(P)(\mathbf{w}_P^H\mathbf{a}(\theta_i)))\mathbf{C}_i^T(\ell)\mathbf{s}\right)\\ \times&\sum_{i=1}^{N_c}\left((\mathbf{v}(1)(\mathbf{w}_1^H\mathbf{a}(\theta_i))+\cdots+\mathbf{v}(P)(\mathbf{w}_P^H\mathbf{a}(\theta_i)))\mathbf{C}_i^T(\ell)\mathbf{s}\right)^H\Bigg\},\end{aligned}$$

since the impulse response of clutter is uncorrelated with each other, Eq. (53) is formulated as

$$\begin{aligned}\bar{\mathbf{R}}_c&=\sum_{i=1}^{N_c}|\beta_i|^2\mathbb{E}\{\mathbf{C}_i^T(\ell)\mathbf{s}\mathbf{s}^H\mathbf{C}_i^*(\ell)\} \qquad (54)\\ &=\sum_{i=1}^{N_c}|\beta_i|^2\sum_{n=-N+1}^{N-1}\sigma_c^2\mathbf{s}_n\mathbf{s}_n^H\\ &=\sum_{i=1}^{N_c}|\beta_i|^2\boldsymbol{\Upsilon},\end{aligned}$$

where $\beta_i=\mathbf{v}(1)\mathbf{w}_1^H\mathbf{a}(\theta_i)+\cdots+\mathbf{v}(P)\mathbf{w}_P^H\mathbf{a}(\theta_i)$.

REFERENCES

[1] L. Zheng, M. Lops, Y. C. Eldar, and X. Wang, "Radar and Communication Coexistence: An Overview: A Review of Recent Methods," *IEEE Signal Processing Magazine*, vol. 36, no. 5, pp. 85–99, 2019.

[2] K. V. Mishra, M. Bhavani Shankar, V. Koivunen, B. Ottersten, and S. A. Vorobyov, "Toward Millimeter-Wave Joint Radar Communications: A Signal Processing Perspective," *IEEE Signal Processing Magazine*, vol. 36, no. 5, pp. 100–114, 2019.

[3] A. Hassanien, M. G. Amin, E. Aboutanios, and B. Himed, "Dual-Function Radar Communication Systems: A Solution to the Spectrum Congestion Problem," *IEEE Signal Processing Magazine*, vol. 36, no. 5, pp. 115–126, 2019.

[4] F. Liu, C. Masouros, A. Li, and T. Ratnarajah, "Robust MIMO Beamforming for Cellular and Radar Coexistence," *IEEE Wireless Communications Letters*, vol. 6, no. 3, pp. 374–377, 2017.

[5] J. Qian, M. Lops, L. Zheng, and X. Wang, "Joint Design for Co-Existence of MIMO Radar and MIMO Communication System," in *2017 51st Asilomar Conference on Signals, Systems, and Computers*, 2017, pp. 568–572.

[6] A. Hassanien, M. G. Amin, Y. D. Zhang, and F. Ahmad, "Signaling Strategies for Dual-Function Radar Communications: An Overview," *IEEE Aerospace and Electronic Systems Magazine*, vol. 31, no. 10, pp. 36–45, 2016.

[7] X. Chen, Z. Feng, Z. Wei, F. Gao, and X. Yuan, "Performance of Joint Sensing-Communication Cooperative Sensing UAV Network," *IEEE Transactions on Vehicular Technology*, vol. 69, no. 12, pp. 15 545–15 556, 2020.

[8] X. Wang, A. Hassanien, and M. G. Amin, "Dual-Function MIMO Radar Communications System Design Via Sparse Array Optimization," *IEEE Transactions on Aerospace and Electronic Systems*, vol. 55, no. 3, pp. 1213–1226, 2019.

[9] F. Liu and C. Masouros, "A Tutorial on Joint Radar and Communication Transmission for Vehicular Networks—Part II: State of the Art and

Challenges Ahead," *IEEE Communications Letters*, vol. 25, no. 2, pp. 327–331, 2021.

[10] ——, "A Tutorial on Joint Radar and Communication Transmission for Vehicular Networks—Part I: Background and Fundamentals," *IEEE Communications Letters*, vol. 25, no. 2, pp. 322–326, 2021.

[11] ——, "A Tutorial on Joint Radar and Communication Transmission for Vehicular Networks—Part III: Predictive Beamforming Without State Models," *IEEE Communications Letters*, vol. 25, no. 2, pp. 332–336, 2021.

[12] D. Ma, N. Shlezinger, T. Huang, Y. Liu, and Y. C. Eldar, "Joint Radar-Communication Strategies for Autonomous Vehicles: Combining Two Key Automotive Technologies," *IEEE Signal Processing Magazine*, vol. 37, no. 4, pp. 85–97, 2020.

[13] A. Hassanien, B. Himed, and M. G. Amin, "Transmit/receive Beamforming Design for Joint Radar and Communication Systems," in *2018 IEEE Radar Conference (RadarConf18)*, 2018, pp. 1481–1486.

[14] A. Hassanien, M. G. Amin, Y. D. Zhang, F. Ahmad, and B. Himed, "Non-coherent PSK-based Dual-Function Radar-Communication Systems," in *2016 IEEE Radar Conference (RadarConf)*, 2016, pp. 1–6.

[15] T. Huang, N. Shlezinger, X. Xu, Y. Liu, and Y. C. Eldar, "MAJoRCom: A Dual-Function Radar Communication System Using Index Modulation," *IEEE Transactions on Signal Processing*, vol. 68, pp. 3423–3438, 2020.

[16] T. Huang, X. Xu, Y. Liu, N. Shlezinger, and Y. C. Eldar, "A Dual-Function Radar Communication System Using Index Modulation," in *2019 IEEE 20th International Workshop on Signal Processing Advances in Wireless Communications (SPAWC)*, 2019, pp. 1–5.

[17] D. Ma, N. Shlezinger, T. Huang, Y. Shavit, M. Namer, Y. Liu, and Y. C. Eldar, "Spatial Modulation for Joint Radar-Communications Systems: Design, Analysis, and Hardware Prototype," *IEEE Transactions on Vehicular Technology*, vol. 70, no. 3, pp. 2283–2298, 2021.

[18] A. Hassanien, M. G. Amin, Y. D. Zhang, and F. Ahmad, "Dual-Function Radar-Communications: Information Embedding Using Sidelobe Control and Waveform Diversity," *IEEE Transactions on Signal Processing*, vol. 64, no. 8, pp. 2168–2181, 2016.

[19] A. Hassanien, Y. D. Zhang, F. Ahmad, and M. G. Amin, "Phase-Modulation Based Dual-Function Radar-Communications," *Iet Radar Sonar & Navigation*, 2017.

[20] A. Ammar, Y. D. Zhang, and Y. Gu, "Dual-Function Radar-Communications Using QAM-based Sidelobe Modulation," *Digital Signal Processing*, vol. 82, pp. 166–174, 2018.

[21] B. Zhao, L. Kong, M. Yang, and G. Cui, "Range-Doppler sidelobe and clutter suppression via time-range adaptive processing," in *Proceedings of 2011 IEEE CIE International Conference on Radar*, vol. 2, 2011, pp. 1809–1812.

[22] S. Blunt and K. Gerlach, "Adaptive Pulse Compression via MMSE Estimation," *IEEE Transactions on Aerospace and Electronic Systems*, vol. 42, no. 2, pp. 572–584, 2006.

[23] T. Higgins, S. D. Blunt, and A. K. Shackelford, "Time-Range Adaptive Processing for pulse agile radar," in *2010 International Waveform Diversity and Design Conference*, 2010, pp. 115–120.

[24] T. Higgins, K. Gerlach, A. K. Shackelford, and S. D. Blunt, "Aspects of Non-Identical Multiple Pulse Compression," in *2011 IEEE RadarCon (RADAR)*, 2011, pp. 895–900.

[25] A. C. O'Connor, J. M. Kantor, and J. Jakabosky, "Joint Equalization Filters that Mitigate Waveform-Diversity Modulation of Clutter," in *2016 IEEE Radar Conference (RadarConf)*, 2016, pp. 1–6.

[26] C. Sahin, J. G. Metcalf, and S. D. Blunt, "Filter Design to Address Range Sidelobe Modulation in Transmit-Encoded Radar-Embedded Communications," in *2017 IEEE Radar Conference (RadarConf)*, 2017, pp. 1509–1514.

[27] S. D. Blunt, M. R. Cook, and J. Stiles, "Embedding Information into Radar Emissions via Waveform Implementation," in *2010 International Waveform Diversity and Design Conference*, 2010, pp. 000 195–000 199.

[28] X. Zhang, X. Wang, and E. Aboutanios, "Effect Analysis of Spatial Modulation on Clutter Mitigation for Joint RadCom Systems and Solutions," in *2020 IEEE Radar Conference (RadarConf20)*, 2020, pp. 1–6.

[29] A. Aubry, A. D. Maio, Y. Huang, and M. Piezzo, "Robust Design of Radar Doppler Filters," *IEEE Transactions on Signal Processing*, vol. 64, no. 22, pp. 5848–5860, 2016.

[30] A. Aubry, A. De Maio, and M. M. Naghsh, "Optimizing Radar Waveform and Doppler Filter Bank via Generalized Fractional Programming," *IEEE Journal of Selected Topics in Signal Processing*, vol. 9, no. 8, pp. 1387–1399, 2015.

[31] M. M. Naghsh, M. Soltanalian, P. Stoica, M. Modarres-Hashemi, A. De Maio, and A. Aubry, "A Doppler Robust Design of Transmit Sequence and Receive Filter in the Presence of Signal-Dependent Interference," *IEEE Transactions on Signal Processing*, vol. 62, no. 4, pp. 772–785, 2014.

[32] X. Du, A. Aubry, A. De Maio, and G. Cui, "Hidden Convexity in Robust Waveform and Receive Filter Bank Optimization Under Range Unambiguous Clutter," *IEEE Signal Processing Letters*, vol. 27, pp. 885–889, 2020.

[33] S. D. Blunt and T. Higgins, "Dimensionality Reduction Techniques for Efficient Adaptive Pulse Compression," *IEEE Transactions on Aerospace and Electronic Systems*, vol. 46, no. 1, pp. 349–362, 2010.

[34] S. Boyd and L. Vandenberghe, *Convex Optimization*. Cambridge University Press, 2009.

[35] L. Z. Bao, "Two-sided Minimum-Variance Distortionless Response Beamformer for MIMO Radar," *Signal Processing*, 2009.

[36] T. A. Apostol, "Mathematical Analysis," *Nature*, vol. 205, no. 4975, 1974.